Int. J. Multiphase Flow Vol. 7, pp. 21–39
Pergamon/Elsevier, 1981. Printed in Great Britain

0301-9322/81/0201-0021/$02.00/0

THE PREDICTION OF STRATIFIED TWO-PHASE FLOW WITH A TWO-EQUATION MODEL OF TURBULENCE

M. AKAI,† A. INOUE and S. AOKI

Research Laboratory for Nuclear Reactors, Tokyo Institute of Technology, Meguro-ku, Tokyo, Japan

(*Received* 23 *August* 1979; *in revised form* 8 *May* 1980)

Abstract—A two-equation model is applied to a stratified two-phase flow system to predict turbulent transport mechanisms in both phases.

In the present analysis, the effects of interfacial waves on the flow field are formulated in terms of boundary conditions for the gas-liquid interface. For the gas phase, the wavy interface has such flow separation effects as a rough surface in a single-phase flow. While for the liquid phase, the waves generate turbulant energy which is transported progressively toward a lower wall region. The analytical results are in good agreement with available data regarding pressure drop, holdup and velocity profiles.

1. INTRODUCTION

Prediction of pressure drop and holdup in stratified two-phase flow is of great importance in many engineering applications. Nuclear reactors, film coolers and oil gas pipelines are the examples of process involving such type of two-phase flow. Recently, this flow or an annular-dispersed flow has been proposed as a cooling system in a controlled fusion reactor. Therefore not only experimental but also analytical studies have been conducted actively. The typical examples of the experimental works can be seen in Hanratty & Engen (1957), Ellis & Gay (1959) or Akai *et al.* (1977). One of the most important results of these studies is that distorted gas velocity profiles have been measured over wavy, rough surfaces. This distortion of the gas velocity profile, i.e. the shift of the plane of maximum velocity toward a smooth upper wall, accompanied with the significant increase in interfacial shear stress have been considered similar to that occurred in rough wall turbulence. We also have studied this flow regime in a horizontal air–mercury system as a basic study for magnetohydrodynamic two-phase flow, and observed the dame phenomena as well as a significant increase in eddy viscosity of the gas phase in the vicinity of the disturbed interface.

The work by Lockhart & Martinelli (1949) is one of the earliest studies to predict analytically the pressure drop and the holdup for stratified two-phase flow. Though this attempt may be the simplest one and applicable to all two-phase flow regimes, relatively low accuracy is attained due to its flexibility. From this point of view, there have been a number of analytical works to predict these characteristics or to improve the Lockhart–Martinelli correlations.

Among these active studies, Johannessen (1972) and Aggour & Sims (1978) presented the relations among non-dimensional pressure drop, ϕ_L or ϕ_G, holdup, 1-α, and the parameter X, giving fairly good agreement with available data. For the wavy interface regime, however, the predicted pressure drops are generally smaller than the measured ones. This underprediction may be due to the lack of consideration about the effects of rough interface on the flow field. We have conducted a semi-empirical analysis which introduced an idea of "wave-induced shear stress", and obtained good results describing the tendency of the pressure drop as well as the distortion of the gas phase velocity profiles. These results are shown in Akai *et al.* (1980).

In the very practical case of turbulent–turbulent flow regime, which the present study treats, the turbulent transport mechanisms in both phases have been described using Blasius friction coefficient formula, 1/7-power law for the velocity profiles or the empirical formula for the eddy viscosity profiles. But when we give our attentions to the development of numerical procedure

†Present address: Thermodynamics Division, Mechanical Engineering Laboratory, Agency of Industrial Science and Technology, Ministry of International Trade and Industry, Tsukuba, Ibaragi, Japan.

for single-phase turbulent shear flows, we could find many successful studies dealing with so called "second order" closures for turbulence equations. This development is a consequence of the need for models of turbulent flow more widely applicable than those incorporating simple notions of effective turbulent coefficients. Jones & Launder (1972, 1973) presented a two-equation model of turbulence which incorporated transport equations for turbulence kinetic energy, k, and energy dissipation rate, ϵ, and expressed the eddy viscosity as a function of these quantities to describe turbulent shear stress. This model was applied to the prediction of laminarization (1972) and low-Reynolds-number phenomena (1973), and has been recognized to give satisfactory results for a variety of flow fields. Hanjalic & Launder (1972, 1976) developed a three-equation model which incorporated Reynolds stress as a dependent variable in addition to k and ϵ, and applied it to an asymmetric flow (1972) and a low-Reynolds-number turbulence (1976).

In such flows with asymmetric velocity profiles as the present case, it has been generally indicated that there exists a displacement between the zeros of the turbulent shear stress ($\overline{u'v'} = 0$), and the mean gradient of the velocity ($\partial u/\partial y = 0$). This means that the turbulence energy production term $-\overline{u'v'}(\partial u/\partial y)$ becomes negative within a zone of the displacement. Of course this phenomena cannot be described by the eddy viscosity hypothesis, and it might be more convenient to use the three-equation model than the two-equation model. In the present analysis, however, we use the two-equation model of turbulence by Jones and Launder with some modifications. For we consider the wavy interface as a turbulence energy source and attempt to treat its effects through the boundary conditions for the turbulence energy. The boundary conditions for the energy dissipation rate can be evaluated from the k-profile. But if we use the three-equation model, it becomes difficult to adopt the boundary conditions for turbulent shear stress because of the complicated structure of the velocity fluctuations or their products in the vicinity of the wavy interface. Moreover, the increase in the number of dependent variables makes the solution procedure complicated and requires long computing times.

The present paper describes the application of the two-equation model of turbulence to the stratified two-phase flow. The purpose of this study is to analyze the flow considering the effects of the interfacial waves on the turbulence structure of both phases. The appropriate boundary conditions for the interface are examined through the comparison with available data and physical considerations.

2. ANALYSIS

The proposed analytical method assumes that the two-phase stratified flow in a rectangular channel should be adequately represented by the two-dimensional flow between two parallel plates. The following fundamental assumptions are made: (1) both fluids are incompressible with constant physical properties, and (2) the flow is steady and fully developed turbulent-turbulent flow. The "steady" assumption in (2) is not introduced in the governing equations described below for computation.

2.1 *Governing equations*

The set of differential equations governing the unsteady turbulent transport process is written in the form:

Streamwise momentum.

$$\frac{\partial u}{\partial t} = \frac{\partial}{\partial y}\left[(\nu + \nu_T)\frac{\partial u}{\partial y}\right] - \frac{1}{\rho}\frac{\partial P}{\partial x}. \qquad [1]$$

Turbulence energy.

$$\frac{\partial k}{\partial t} = \frac{\partial}{\partial y}\left[(\nu + \nu_T)\frac{\partial k}{\partial y}\right] + \nu_T\left(\frac{\partial u}{\partial y}\right)^2 - \epsilon. \qquad [2]$$

Energy dissipation.

$$\frac{\partial \epsilon}{\partial t} = \frac{\partial}{\partial y}\left[\left(\nu + \frac{\nu_T}{\sigma_\epsilon}\right)\frac{\partial \epsilon}{\partial y}\right] + C_1 f_1 \frac{\epsilon}{k}\nu_T\left(\frac{\partial u}{\partial y}\right)^2 - C_2 f_2 \frac{\epsilon\tilde{\epsilon}}{k} + 2\nu\nu_T\left(\frac{\partial^2 u}{\partial y^2}\right)^2. \quad [3]$$

Turbulent viscosity hypothesis.

$$-\overline{u'v'} = \nu_T \frac{\partial u}{\partial y} = C_\mu f_\mu \frac{k^2}{\epsilon}\frac{\partial u}{\partial y}, \quad [4]$$

where u, k, ϵ and P denote mean streamwise velocity, turbulent kinetic energy, turbulent energy dissipation rate and static pressure respectively, and x is Cartesian space coordinate in the mean flow direction, y is the coordinate normal to the wall. Equations [2]–[4] represent the two-equation model of turbulence proposed by Jones & Launder (1972, 1973). In the present study, some modifications have been made to the original set of equations. These considerations are mainly based on the work by Hanjalic & Launder (1972, 1976) in which they treated an asymmetric turbulent flow between parallel plates and low-Reynolds-number turbulence.

The main feature of these modifications is to introduce the quantity $\tilde{\epsilon}$ and replacing ϵ^2 in the original dissipation equation by $\epsilon\tilde{\epsilon}$. The quantity $\tilde{\epsilon}$ is defined as

$$\tilde{\epsilon} = \epsilon - 2\nu\left(\frac{\partial\sqrt{(k)}}{\partial y}\right)^2 \quad [5]$$

and represents the "isotropic" part of the dissipation rate. In the original turbulent model equations (Jones & Launder 1973), a term of the form

$$2\nu\left(\frac{\partial\sqrt{(k)}}{\partial y}\right)^2$$

was added to the right of [2]. They included this term for computational purpose to let ϵ go to zero at the wall. This boundary condition for ϵ is necessary for their finite-difference procedure to solve the ϵ-equation; they introduced this extra term which described the actual isotropic behavior of the turbulence dissipation rate in the immediate vicinity of the wall, and which was of negligible magnitude in a core region of the flow. In the present analysis this term has been excluded from [2], while the quantity $\tilde{\epsilon}$ has been introduced as described above. Consequently, the boundary condition for the energy dissipation rate becomes

$$\epsilon \to 2\nu\left(\frac{\partial\sqrt{(k)}}{\partial y}\right)^2 \text{ for } y \to 0$$

instead of $\epsilon \to 0$, which has poor physical appropriateness.

The model equations contain four empirical constants, C's and σ_ϵ, which are assigned the values given in table 1. The influence of the turbulent Reynolds number $R_T = k^2/\epsilon\nu$ is introduced by f's summarised in table 2.

2.2 *Formulation for stratified two-phase flow between parallel plates*

In this section we adopt the above set of turbulence model equations to the co-current, stratified, two-phase flow between parallel plates. The following nondimensional variables are

Table 1. Empirical constants in model equations

C_μ	C_1	C_2	σ_ϵ
0.09	1.45	2.0	1.3

Table 2. Reynolds-number functions in model equations

f_1	1.0
f_2	$1.0-0.3\exp(-R_T^2)$
f_μ	$\exp[-2.5/(1+R_T/50)]$

introduced:

$$u=\frac{bu_*^2}{\nu_L}\tilde{u},\quad k=u_*^2E,\quad \epsilon=\frac{u_*^4}{\nu_L}D,\quad P=\rho_L\frac{u_*^4}{\nu_L^2}b^2\tilde{P},$$

$$y=b\tilde{y},\quad x=b\tilde{x},\quad t=\frac{\nu_L}{u_*^2}\tilde{t},$$

$$\mathrm{Re}=\frac{u_*b}{\nu_L},$$

where b denotes the distance between parallel plates, and u_* is the friction velocity defined by the shear stress at the lower wall and the density of the liquid. The liquid properties (subscript "L") are selected as scaling parameters. In these expressions, the tilde quantities, E and D are dimensionless. We drop the tildes for convenience, but henceforth in the paper all quantities are dimensionless unless stated otherwise.

With above dimensionless quantities, we can write the coupled equations for two phases as follows:

Momentum for liquid phase.

$$\frac{\partial u_L}{\partial t}=\frac{1}{\mathrm{Re}^2}\frac{\partial}{\partial y}\left[\left(1+C_\mu f_\mu\frac{E_L^2}{D_L}\right)\frac{\partial u_L}{\partial y}\right]-\frac{\partial P}{\partial x}. \tag{6}$$

Momentum for gas phase.

$$\frac{\partial u_G}{\partial t}=\frac{\nu_G}{\nu_L}\frac{1}{\mathrm{Re}^2}\frac{\partial}{\partial y}\left[\left(1+\frac{\nu_L}{\nu_G}C\mu f\mu\frac{E_G^2}{D_G}\right)\frac{\partial u_G}{\partial y}\right]-\frac{\rho_L}{\rho_G}\frac{\partial P}{\partial x}. \tag{7}$$

Turbulence energy for liquid phase.

$$\frac{\partial E_L}{\partial t}=\frac{1}{\mathrm{Re}^2}\frac{\partial}{\partial y}\left[\left(1+C_\mu f_\mu\frac{E_L^2}{D_L}\right)\frac{\partial E_L}{\partial y}\right]+C_\mu f_\mu\frac{E_L^2}{D_L}\left(\frac{\partial u_L}{\partial y}\right)^2-D_L. \tag{8}$$

Turbulence energy for gas phase.

$$\frac{\partial E_G}{\partial t}=\frac{\nu_G}{\nu_L}\frac{1}{\mathrm{Re}^2}\frac{\partial}{\partial y}\left[\left(1+\frac{\nu_L}{\nu_G}C_\mu f_\mu\frac{E_G^2}{D_G}\right)\frac{\partial E_G}{\partial y}\right]+C_\mu f_\mu\frac{E_G^2}{D_G}\left(\frac{\partial u_G}{\partial y}\right)^2-D_G. \tag{9}$$

Energy dissipation for liquid phase.

$$\begin{aligned}\frac{\partial D_L}{\partial t}=&\frac{1}{\mathrm{Re}^2}\frac{\partial}{\partial y}\left[\left(1+\frac{1}{\sigma_\epsilon}C_\mu f_\mu\frac{E_L^2}{D_L}\right)\frac{\partial E_L}{\partial y}\right]+C_1C_\mu f_\mu E_L\left(\frac{\partial u_L}{\partial y}\right)^2\\&-C_2f_2\frac{D_L\tilde{D}_L}{E_L}+2.0\frac{1}{\mathrm{Re}^2}C_\mu f_\mu\frac{E_L^2}{D_L}\left(\frac{\partial^2u_L}{\partial y^2}\right)^2,\\ \tilde{D}_L=&D_L-2.0\frac{1}{\mathrm{Re}^2}\left(\frac{\partial\sqrt{(E_L)}}{\partial y}\right)^2.\end{aligned} \tag{10}$$

Energy dissipation for gas phase.

$$\frac{\partial D_G}{\partial y} = \frac{\nu_G}{\nu_L}\frac{1}{\mathrm{Re}^2}\frac{\partial}{\partial y}\left[\left(1+\frac{\nu_L}{\nu_G}\frac{1}{\sigma_\epsilon}C_\mu f_\mu \frac{E_G^2}{D_G}\right)\frac{\partial D_G}{\partial y}\right] + C_1 C_\mu f_\mu E_G\left(\frac{\partial u_G}{\partial y}\right)^2$$
$$- C_2 f_2 \frac{D_G \tilde{D}_G}{E_G} + 2.0\frac{\nu_G}{\nu_L}\frac{1}{\mathrm{Re}^2}C_\mu f_\mu \frac{E_G^2}{D_G}\left(\frac{\partial^2 u_G}{\partial y^2}\right)^2, \qquad [11]$$
$$\tilde{D}_G = D_G - 2.0\frac{\nu_G}{\nu_L}\frac{1}{\mathrm{Re}^2}\left(\frac{\partial\sqrt{(E_G)}}{\partial y}\right)^2,$$

and the turbulent Reynolds numbers are:

$$R_{TL} = \frac{E_L^2}{D_L} \quad \text{(liquid phase)},$$

$$R_{TG} = \frac{\nu_L}{\nu_G}\frac{E_G^2}{D_G} \quad \text{(gas phase)}.$$

In above equations, the subscripts "L" and "G" refer to the liquid and the gas phase respectively.

We incorporate the following boundary conditions for the lower and the upper wall:

$$u_L = 0, \quad E_L = 0, \quad D_L = 2\frac{1}{\mathrm{Re}^2}\left(\frac{\partial\sqrt{(E_L)}}{\partial y}\right)^2 \text{ at } y = 0$$
$$u_G = 0, \quad E_G = 0, \; D_G = 2\frac{\nu_G}{\nu_L}\frac{1}{\mathrm{Re}^2}\left(\frac{\partial\sqrt{(E_G)}}{\partial y}\right)^2 \text{ at } y = 1. \qquad [12]$$

Moreover the boundary conditions for the gas–liquid interface are necessary. Here, for the basic case in which the gas–liquid interface is assumed to be smooth, the appropriate boundary conditions are as follows:

at $y = y_i$;

$$u_L = u_G, \; \tau_L = \tau_G,$$
$$E_L = 0, \; E_G = 0,$$
$$D_L = 2\frac{1}{\mathrm{Re}^2}\left(\frac{\partial\sqrt{(E_L)}}{\partial y}\right)^2, \; D_G = 2\frac{\nu_G}{\nu_L}\frac{1}{\mathrm{Re}^2}\left(\frac{\partial\sqrt{(E_G)}}{\partial y}\right)^2. \qquad [13]$$

These boundary conditions are, of course, necessary to be modified when they are applied to the wavy interface. This consideration will be given in later sections.

3.3 *Solution procedure*

In the present analysis, the required results are the fully developed and steady state characteristics of the two-phase flow, i.e. the pressure drop, the liquid film thickness or the velocity field. So, the numerical calculation involves an unsteady approach sequence of solutions for the finite difference versions of [6]–[11]. This sequence is similar to that introduced by Daly & Harlow (1970), and traces the development of the flow through time from the initial state to the steady state.

In this type of analysis, it is convenient for us to obtain the solution under the condition in which the volumetric flow rate of the gas phase, Q_G, and that of the liquid phase, Q_L, are given. This requirement is easily satisfied if we use the von Mises transformation (Ames 1965) to

accomplish the mathematical formulations for [6]–[11]. Though we first used this method for the numerical analysis, this procedure required an enormous computing time for a run. This unsuccessful result is mainly due to the large difference between Q_L and Q_G of order 10^2, which causes the large difference between corresponding stream functions. Therefore the cell sizes for both phases become unbalanced and this results in a severe condition for convergence. Another problem existed in the sequence of solving the momentum equations simultaneously by the unsteady approach method, because it needed additional corrections regarding the streamwise pressure gradient.

From these points of view, we developed a new sequence which involves unsteady solutions for E- and D-equations and steady state solutions for the momentum equations.

Solution of steady state momentum equations

Consider the steady state of the momentum equations [6] and [7] in which the profiles of E and D are given as an initial condition. Then the momentum equations are rewritten as follows:

For liquid phase $0 \le y \le y_i$.

$$\mathrm{Re}^2 \frac{\partial P}{\partial x} = \frac{\partial}{\partial y} \tau_L, \tag{14}$$

$$\tau_L = \left(1 + C_\mu f_\mu \frac{E_L^2}{D_L}\right) \frac{\partial u_L}{\partial y} \equiv F_L \frac{\partial u_L}{\partial y}, \tag{15}$$

For gas phase $y_i \le y \le 1$.

$$\mathrm{Re}^2 \frac{\partial P}{\partial x} = \frac{\partial}{\partial y} \tau_G, \tag{16}$$

$$\tau_G = \frac{\mu_G}{\mu_L}\left(1 + \frac{\nu_L}{\nu_G} C_\mu f_\mu \frac{E_G^2}{D_G}\right) \frac{\partial u_G}{\partial y} \equiv F_G \frac{\partial u_G}{\partial y}. \tag{17}$$

Here we introduce a new coordinate η for the gas phase which is defined as

$$1 - y = \eta. \tag{18}$$

Then the momentum equation for the gas phase becomes

$$\mathrm{Re}^2 \frac{\partial P}{\partial x} = -\frac{\partial}{\partial \eta} \tau_G \qquad \text{for } 0 \le \eta \le \eta_i, \tag{19}$$

$$\tau_G = -\frac{\mu_G}{\mu_L}\left(1 + \frac{\nu_L}{\nu_G} C_\mu f_\mu \frac{E_G^2}{D_G}\right) \frac{\partial u_G}{\partial \eta} \equiv -F_G \frac{\partial u_G}{\partial \eta}. \tag{20}$$

In [15], E goes to zero at the wall while D remains to have a finite value, then the nondimensional shear stress at the lower wall becomes

$$\tau_L(0) = \left.\frac{\partial u_L}{\partial y}\right|_{y=0} = 1,$$

from the definitions. Consequently, integration of [14] yields the shear stress distribution in the liquid phase as

$$\tau_L(y) = 1 + \mathrm{Re}^2 \frac{\partial P}{\partial x} y \quad (0 \le y \le y_i). \tag{21}$$

In the same way, the shear stress distribution in the gas phase is obtained from [16] as follows:

$$\tau_G(\eta) = \tau_1 - \mathrm{Re}^2 \frac{\partial P}{\partial x} \eta \quad (0 \le \eta \le \eta_i), \tag{22}$$

where τ_1 denotes the upper wall shear stress. From the continuity of the shear stress at the interface $[\tau_G(\eta_i) = \tau_L(y_i)]$,

$$\tau_1 = 1 + \mathrm{Re}^2 \frac{\partial P}{\partial x}. \tag{23}$$

From [15] and [21], we obtain the velocity profile in the liquid phase as

$$u_L(y) = \int_0^y \frac{1}{F_L} \mathrm{d}y + \mathrm{Re}^2 \frac{\partial P}{\partial x} \int_0^y \frac{1}{F_L} y \, \mathrm{d}y, \tag{24}$$

and from [20] and [22], the gas phase velocity profile yields

$$u_G(\eta) = -\tau_1 \int_0^\eta \frac{1}{F_G} \mathrm{d}\eta + \mathrm{Re}^2 \frac{\partial p}{\partial x} \int_0^\eta \frac{1}{F_G} \eta \, \mathrm{d}\eta. \tag{25}$$

Considering the continuity of the velocity of the gas and the liquid phase at the interface, it follows that

$$\int_0^{y_i} \frac{1}{F_L} \mathrm{d}y + \mathrm{Re}^2 \frac{\partial P}{\partial x} \int_0^{y_i} \frac{1}{F_L} y \, \mathrm{d}y = -\tau_1 \int_0^{\eta_i} \frac{1}{F_G} \mathrm{d}\eta + \mathrm{Re}^2 \frac{\partial P}{\partial x} \int_0^{\eta_i} \frac{1}{F_G} \eta \, \mathrm{d}\eta. \tag{26}$$

When volumetric flow rates per unit width for both phases, Q_L and Q_G, are given, the film Reynolds numbers can be defined as

$$\mathrm{Re}_L = \frac{\overline{u_L}\,\delta}{\nu_L} = \frac{Q_L}{\nu_L}, \quad \mathrm{Re}_G = \frac{\overline{u_G}(b-\delta)}{\nu_G} = \frac{Q_G}{\nu_G},$$

where $\overline{u_L}$ and $\overline{u_G}$ are the (dimensional) mean velocity of the liquid and the gas phase respectively, and δ is the liquid film thickness. Q_L and Q_G can be expressed in terms of integrals of the nondimensional velocity profiles so that the Reynolds numbers are written of the form

$$\mathrm{Re}_L = \mathrm{Re}^2 \int_0^{y_i} u_L(y) \, \mathrm{d}y, \tag{27}$$

$$\mathrm{Re}_G = \frac{\nu_L}{\nu_G} \mathrm{Re}^2 \int_0^{\eta_i} u_G(\eta) \, \mathrm{d}\eta. \tag{28}$$

Substituting [24] into [27], and [25] into [28], we obtain

$$\frac{\mathrm{Re}_L}{\mathrm{Re}^2} = \int_0^{y_i} \int_0^y \frac{1}{F_L} \mathrm{d}y \, \mathrm{d}y + \mathrm{Re}^2 \frac{\partial P}{\partial x} \int_0^{y_i} \int_0^y \frac{1}{F_L} y \, \mathrm{d}y \, \mathrm{d}y, \tag{29}$$

$$\frac{\nu_G}{\nu_L} \frac{\mathrm{Re}_G}{\mathrm{Re}^2} = -\tau_1 \int_0^{\eta_i} \int_0^\eta \frac{1}{F_G} \mathrm{d}\eta \, \mathrm{d}\eta + \mathrm{Re}^2 \int_0^{\eta_i} \int_0^\eta \frac{1}{F_G} \eta \, \mathrm{d}\eta \, \mathrm{d}\eta. \tag{30}$$

And from [18],

$$\eta_i + y_i = 1 . \qquad [31]$$

Equations [23], [26], [29], [30] and [31] for the given profiles of $F_L(y)$ and $F_G(\eta)$ may be solved to obtain five unknown parameters: τ_1, Re, $\partial P/\partial x$, y_i and η_i. It is difficult, however, to solve these equations since the unknown variables y_i and η_i have come to be integral limits in [26], [29] and [30].

In order to eliminate this difficulty, we introduce new (stretching) coordinates defined by

$$F_L(y) = F_{L\text{old}}\left(\frac{y_{i\text{old}}}{y_i} y\right) \equiv F_{L\text{old}}(\xi) , \qquad [32]$$

$$F_G(\eta) = F_{G\text{old}}\left(\frac{\eta_{i\text{old}}}{\eta_i} \eta\right) \equiv F_{G\text{old}}(\zeta) , \qquad [33]$$

where the subscript "old" denotes that these quantities are the trial values or the values obtained in the up-to-date step. Equations [32] and [33] mean that the total (molecular+ turbulent) viscosity profiles may be assumed to be only stretching along y-coordinate and not change their magnitude by the change or the correction of the liquid film thickness. This is, of course, not true since the significant change in liquid film thickness may cause a serious effect on the entire flow field. But as the solution is approaching to the steady state, the change of the liquid film thickness becomes small, indeed so small that no effect on the flow field, i.e. the velocity profiles, turbulence energy profiles, pressure drop, etc. can be distinguished. Using these new variables, the definite integrals in [26], [29] and [30] can be rewritten, for example, as follows:

$$\int_0^{y_i} \frac{1}{F_L(y)} \mathrm{d}y = \frac{y_i}{y_{i\text{old}}} \int_0^{y_{i\text{old}}} \frac{1}{F_{L\text{old}}(\xi)} \mathrm{d}\xi .$$

The integral of the left can be calculated by a numerical integration of "old" value of $1/F_L$ over the liquid phase.

Consequently, [26], [29] and [30] are rewritten as

$$\left(\frac{y_i}{y_{i\text{old}}}\right)\bar{\phi}_L + \tau_1\left(\frac{\eta_i}{\eta_{i\text{old}}}\right)\bar{\phi}_G$$
$$= \mathrm{Re}^2 \frac{\partial P}{\partial x}\left[-\left(\frac{y_i}{y_{i\text{old}}}\right)^2 \bar{\psi}_L + \left(\frac{\eta_i}{\eta_{i\text{old}}}\right)^2 \bar{\psi}_G \right], \qquad [34]$$

$$\frac{\mathrm{Re}_L}{\mathrm{Re}^2} = \left(\frac{y_i}{y_{i\text{old}}}\right)^2 \Gamma_L + \mathrm{Re}^2 \frac{\partial P}{\partial x}\left(\frac{y_i}{y_{i\text{old}}}\right)^3 \Lambda_L , \qquad [35]$$

$$\frac{\nu_G}{\nu_L}\frac{\mathrm{Re}_G}{\mathrm{Re}^2} = -\tau_1\left(\frac{\eta_i}{\eta_{i\text{old}}}\right)^2 \Gamma_G + \mathrm{Re}^2 \frac{\partial P}{\partial x}\left(\frac{\eta_i}{\eta_{i\text{old}}}\right)^3 \Lambda_G , \qquad [36]$$

where

$$\bar{\phi}_L \equiv \phi_L(y_{i\text{old}}) = \int_0^{y_{i\text{old}}} \frac{1}{F_{L\text{old}}(\xi)} \mathrm{d}\xi ,$$

$$\bar{\phi}_G \equiv \phi_G(\eta_{i\text{old}}) = \int_0^{\eta_{i\text{old}}} \frac{1}{F_{G\text{old}}(\zeta)} \mathrm{d}\zeta ,$$

$$\bar{\psi}_L \equiv \psi_L(y_{i\text{old}}) = \int_0^{y_{i\text{old}}} \frac{1}{F_{L\text{old}}(\xi)} \xi \, d\xi,$$

$$\bar{\psi}_G \equiv \psi_G(\eta_{i\text{old}}) = \int_0^{\eta_{i\text{old}}} \frac{1}{F_{G\text{old}}(\zeta)} \zeta \, d\zeta,$$

$$\Gamma_L \equiv \int_0^{y_{i\text{old}}} \int_0^{\xi} \frac{1}{F_{L\text{old}}(\xi)} d\xi \, d\xi = \int_0^{y_{i\text{old}}} \phi_L(\xi) \, d\xi,$$

$$\Gamma_G \equiv \int_0^{\eta_{i\text{old}}} \int_0^{\zeta} \frac{1}{F_{G\text{old}}(\zeta)} d\zeta \, d\zeta = \int_0^{\eta_{i\text{old}}} \phi_G(\zeta) \, d\zeta,$$

$$\Lambda_L \equiv \int_0^{y_{i\text{old}}} \int_0^{\xi} \frac{1}{F_{L\text{old}}(\xi)} \xi \, d\xi \, d\xi = \int_0^{y_{i\text{old}}} \psi_L(\xi) \, d\xi,$$

$$\Lambda_G \equiv \int_0^{\eta_{i\text{old}}} \int_0^{\zeta} \frac{1}{F_{G\text{old}}(\zeta)} \zeta \, d\zeta \, d\zeta = \int_0^{\eta_{i\text{old}}} \psi_G(\zeta) \, d\zeta.$$

Equations [23], [31], [34], [35] and [36] constitute an explicit form regarding τ_1, Re, $\partial P/\partial x$, y_i and η_i. There equations are manipulated to yield

$$\begin{aligned}
&[(XG + XE)(XD - XC) - (XB - XA)(XH + XF)]\,\eta_i^4 \\
&+ [(XB - XA)(XG + 3XF) - 2XE(XD - XC) - XA(XH + XF) \\
&\qquad - (XG + XE)(XB - 2XC)]\,\eta_i^3 \\
&+ [2XE(XB - 2XC) - XC(XG + XE) + XE(XD - XC) - 3XF(XB - XA) \\
&\qquad + XA(XG + 3XF)]\,\eta_i^2 \\
&+ [XF(XB - XA) - 3XA \cdot XF + 2XC \cdot XE - XE(XB - 2XC)]\,\eta_i \\
&+ XA \cdot XF - XC \cdot XE \\
&= 0,
\end{aligned} \qquad [37]$$

where

$$XA = \frac{\bar{\phi}_L}{y_{i\text{old}}}, \quad XB = \frac{\bar{\phi}_G}{\eta_{i\text{old}}}, \quad XC = \frac{\bar{\psi}_L}{y_{i\text{old}}}, \quad XD = \frac{\bar{\psi}_G}{\eta_{i\text{old}}},$$

$$XE = \frac{\Gamma_L}{y_{i\text{old}^2}}, \quad XF = \frac{\Lambda_L}{y_{i\text{old}^3}}, \quad XG = \frac{\nu_L}{\nu_G} \frac{\mathrm{Re}_L}{\mathrm{Re}_G} \frac{\Gamma_G}{\eta_{i\text{old}^2}^2}, \quad XH = \frac{\nu_L}{\nu_G} \frac{\mathrm{Re}_L}{\mathrm{Re}_G} \frac{\Lambda_G}{\eta_{i\text{old}^3}^3},$$

This fourth order equation for η_i can be solved algebraically, but we use a numerical procedure (bisection method) for convenience. It was confirmed that, for a given flow condition, [37] had a unique solution in the range $0 < \eta_i < 1$. If we first find out the solution for η_i, then a set of the corresponding values for y_i, τ_1, Re and $\partial P/\partial x$ is obtained easily from the other equations. Then the velocity profiles for both phases can be calculated from [24] and [25] as follows:

$$u_L(y) = \frac{y_i}{y_{i\text{old}}} \phi_L(\xi) + \mathrm{Re}^2 \frac{\partial P}{\partial x} \left(\frac{y_i}{y_{i\text{old}}} \right)^2 \psi_L(\xi), \qquad [38]$$

$$u_G(\eta) = -\tau_1 \frac{\eta_i}{\eta_{i\text{old}}} \phi_G(\zeta) + \mathrm{Re}^2 \frac{\partial P}{\partial x} \left(\frac{\eta_i}{\eta_{i\text{old}}} \right)^2 \psi_G(\zeta). \qquad [39]$$

Solution of E- *and* D-*equations*

As mentioned before, the turbulent energy and the energy dissipation equations are solved by the unsteady approach method. During each calculation cycle we first solve the momentum equations to obtain u-profile, and then solve the unsteady E- and D-equations. Equations

[8]–[11] have analogous parabolic forms and are written schematically as

$$\frac{\partial q}{\partial t} = \{\text{diffusion} + \text{production} + \text{dissipation}\}, \qquad [40]$$

where q denotes the corresponding variable, E or D. Here the simple, forward-step, finite difference equations of the form,

$$\frac{q_{\text{new}} - q_{\text{old}}}{\delta t} = \{\text{diffusion} + \text{production} + \text{dissipation}\}_{\text{old}}, \qquad [41]$$

are incorporated to solve the unsteady equations of the form [40], where δt denotes the time increment. When the explicit form of a finite difference equation is used, the stability condition for the formula becomes an important problem. As is widely known (e.g. Ames 1965), the stability of this scheme mainly depends on the form of the non-linear diffusion term such as

$$\frac{\partial}{\partial y}\left[K(q)\frac{\partial q}{\partial y}\right],$$

or in the finite difference form,

$$\frac{\delta}{\delta y}\left[K(q)\frac{\delta q}{\delta y}\right], \qquad [42]$$

where $K(q)$ is a diffusion coefficient and, in the present case, this represents the total viscosity for the turbulence energy or the energy dissipation rate.

The stability condition for this scheme is expressed as follows:

$$\frac{K(q)\cdot \delta t}{(\delta y)^2} < \frac{1}{2}.$$

In the present numerical treatment, the time increment δt is determined in each cycle as

$$\delta t = \frac{1}{4}\frac{\min[\delta y^2, \delta \eta^2]}{\max[K_L(y), K_G(\eta)]}.$$

Moreover, an additional care has been taken for this term, i.e. it is more accurate to use a non-conservation form,

$$\frac{\partial}{\partial y}\left[K(q)\frac{\partial}{\partial y}\right] \Rightarrow K(q)\frac{\delta^2 q}{\delta y^2} + \frac{\delta K(q)}{\delta y}\frac{\delta q}{\delta y},$$

than to use a conservation form as expressed in [42]. Taking into account these considerations, the resulted numerical process has been always stable and a satisfactory convergence is obtained.

The criterion used to determine whether a problem has converged sufficiently to the steady state is that

$$\max\left[\frac{\sum\left|\frac{\delta E_L}{\delta t}\right|^2}{\sum E_L^2}, \frac{\sum\left|\frac{\delta E_G}{\delta t}\right|^2}{\sum E_G^2}, \frac{\sum\left|\frac{\delta D_L}{\delta t}\right|^2}{\sum D_L^2}, \frac{\sum\left|\frac{\delta D_G}{\delta t}\right|^2}{\sum D_G^2}\right] < 10^{-8},$$

where the summations being taken over the corresponding phase. A reduction in the numerical value in the criterion to 10^{-10} had an insignificant effect on the final results.

Initial conditions

As described in the previous sections, initial profiles for E_L, E_G, D_L and D_G and a trial value for y_i (or η_i) are necessary as starting conditions. Of course it is preferable to choose these conditions to roughly approximate the expected steady state profiles in order to reduce the computing time. Unfortunately, however, the available information regarding the turbulence structure for this type of flow is poor. So, at the preliminary stage of the calculation, the initial profiles for the turbulence energy and the energy dissipation rate were provided numerically from the analogy to a single-phase turbulent flow. This calculation was, of course, an inefficient one as to computing time, but provided useful starting conditions to the subsequent calculations. The actual numerical analysis has been conducted using the numerical results of this preliminary calculation or of the preceding analysis having the close value of input condition, i.e. Q_L and Q_G. The trial value of y_i is not a serious problem regarding the convergence, so we use $y_i = 0.3$ as a starting value.

150 cross-stream nodes were used first with two thirds of these covering the gas phase, and subsequently they were reduced to 70, with 50 for the gas phase, to reduce the computation time. This change in cell size, however, appeared to cause no significant discrepancy between the results. For a mesh of 70 cells and appropriate initial conditions, generally, about 10^4 calculation cycles are necessary to reach steady state, leading to computing times per a run of about 120 sec on the HITAC M-180 computer at Tokyo Institute of Technology.

3. RESULTS AND DISCUSSIONS

In this section the numerical results for two types of boundary conditions (smooth interface and wavy interface) are shown and compared with the data of stratified air-mercury flow in a horizontal rectangular channel. The internal dimensions of the test channel were 48 mm wide and 18 mm high, with the total length 3.6 m. The details of the experiment is shown in Akai *et al.* (1980). In addition to the results described in the above paper, we have measured the mean velocity profile and the streamwise turbulence intensity profiles in the mercury film flow. These velocity data were obtained using wedge-shaped hot-film probes (DISA 55R36) with overheating about 5°C. These probes were traversed vertically by a micrometer head with ±0.02 mm of accuracy. The region very close to the lower wall could not be measured because of the size of the probe. The closest approach was $y = 1.1$ mm. Also the region near the gas-liquid interface could not be accessed, for the high surface tension of the mercury causes the probe to be exposed to the air flow. The output signals from the anemometer were processed in terms of probability density functions to determine the mean and the fluctuating voltages. The resulted mean voltage profile was integrated over the liquid film to obtain the average voltage corresponding to the average velocity. The calibration curve for the anemometer could be determined by repeating this procedure for various gas or liquid flow rates. There are two possible causes for the error in this calibration method, i.e. the velocity profile in the wide direction and the lack of the velocity data near the lower wall and the interface. Although this source might introduce some errors in estimating a point velocity, the resulant shapes of the mean velocity or the turbulence intensity profiles should be considered not to change seriously.

The analysis of the turbulent air flow was conducted prior to the stratified flow calculation to confirm that the modifications to the equations or the boundary conditions should be reasonable. The calculated friction coefficient $C_f = \tau_0/(1/2)\,\rho\bar{u}^2)$ is shown in figure 1 with our experimental data obtained in the test channel described above. As can be seen in the figure, the predicted value for C_f is slightly smaller than the experimental results. This tendency may be partly due to the small aspect ratio of the channel, which is inconsistent to the assumption of two-dimensional flow. But the discrepancy of these values (a few per cent) is small enough that we consider the present equations and the boundary conditions to be sufficient.

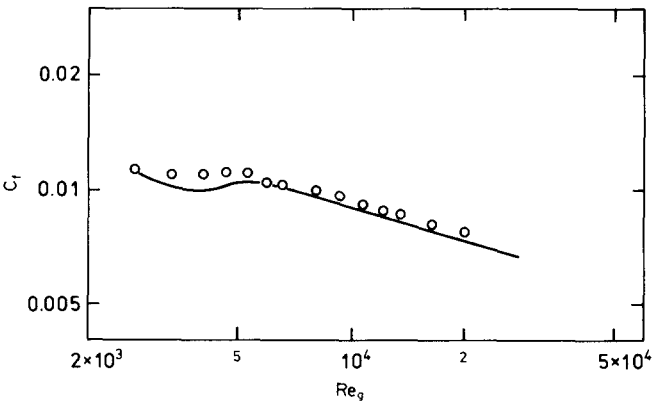

Figure 1. Friction coefficient of air flow. ○, Experiment; —, prediction.

Henceforth in this section the analytical results for the stratified flow will be compared to the experimental data at $Re_L = 8.04 \times 10^3$.

3.1 *Smooth interface case*

In this case, the numerical calculation has been conducted under the boundary condition [13]. The results for the pressure drop and the holdup are presented in terms of the Lockhart–Martinelli parameters in figures 2 and 3. In these figures, $X_{tt}^2 = (dP/dx)_L/(dP/dx)_G$ is the ratio of the frictional pressure drop of the liquid phase to that of the gas phase when each phase flows alone in the channel, and $\phi_L^2 = (dP/dx)_{TP}/(dP/dx)_L$ is the ratio of the two-phase flow pressure drop to the pressure drop of the liquid phase flowing alone in the channel. The solid lines show the results of the present analysis and the dashed lines give the correlations for turbulent–turbulent flow by Aggour & Sims (1978) which are of the form,

$$X_{tt} = 1.189(1-\alpha)^2(2-\alpha)/\alpha^3,$$
$$\phi_L^2 = 0.841/(1-\alpha)^2(2-\alpha), \qquad [43]$$

where α is the void fraction or $1 - \delta/b$. Aggour and Sims derived more complicated relations through the analysis of gas–liquid stratified flow between two wide parallel plates taking into account the interfacial shear stress and a smooth, moving interface. They simplified those equations under the condition $(Q_L/Q_G)[\alpha/(1-\alpha)] \ll 1$ to yield the relations [43]. These cor-

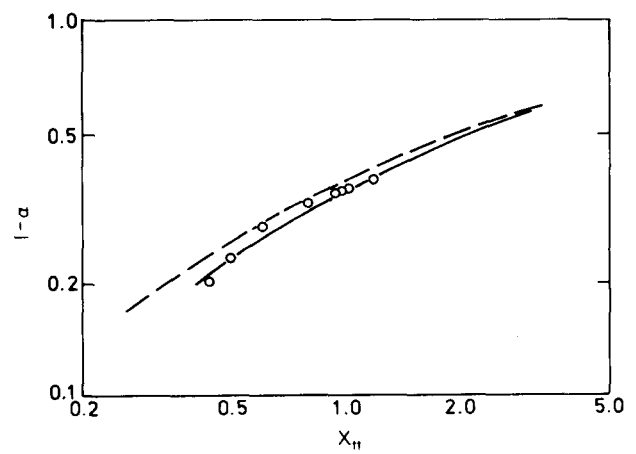

Figure 2. Holdup for air-mercury flow. $Re_L = 8.04 \times 10^3$. ○, Experiment; —, prediction (smooth interface); - - -, correlation by Aggour and Sims.

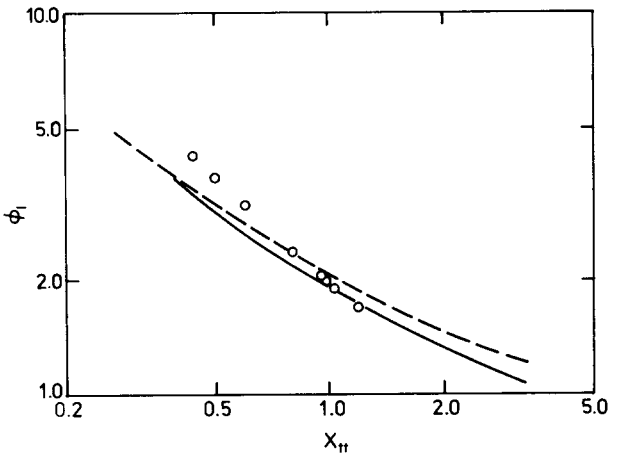

Figure 3. Non-dimensional pressure drop for air–mercury flow. $Re_L = 8.04 \times 10^3$. O, Experiment; —, prediction (smooth interface); - - -, correlation by Aggour and Sims.

relations can be derived directly using the assumption that the interfacial velocity is negligible for the gas phase, i.e. the shear stress at the interface is equal to that at the upper wall. In those flow conditions, i.e. when Re_L is small, the present analysis shows closer tendency to [43], and for $Re_L < 4 \times 10^3$, the results cannot be distinguished from the dashed lines. This fact indicates that the present solution procedure for the stratified flow should be appropriate.

The experimental value especially for the pressure drop has a tendency to deviate from the analytical curve for the smooth interface case as the gas flow rate is increased ($X_{tt}^2 \to 0$). This is a natural result of disregarding the effect of the rough interface.

3.2 *Wavy interface case*

As mentioned in the previous sections, we intend to treat the effects of the interfacial waves on the flow field through considerations about the boundary conditions at the interface. There may be one possible expression for this effect, e.g. to consider the waves as a turbulence energy source. The simplest approach for this concept is to give k_L and k_G some finite values at the interface as the boundary condition. These values can be evaluated from the wave structures. With a simple consideration the perturbation energy at the interface can be written as

$$k_i = \beta \times \left(\frac{2\Delta h}{T}\right)^2, \qquad [44]$$

where Δh and T denote the wave height and the wave period respectively and β is a numerical constant. Equation [44] means that the turbulence energy at the interface can be represented by the surface displacement velocity in the vertical direction. The boundary condition for the turbulence energy at the interface is given by

$$k_L = k_G = k_i. \qquad [45]$$

But we have not reached satisfactory results using [45] only. This is because that, though the magnitude of k_i (when $\beta \simeq 1$) has the same order to the turbulence energy in the bulk liquid flow, it is too small to influence the flow structure of the gas phase.

This problem might be resolved if one considers that the rough wavy interface causes the separation of the gas flow above it. In this case, the continuity condition for the turbulence energy at the interface may not always be necessary. Large scale eddies containing a large amount of energy are produced by the flow separation. This process is considered to be not concerned with the turbulence structures in the liquid phase. In these circumstances, however,

it may be reasonable to expect that the microscopic relationship between the turbulence energy and the energy dissipation rate should hold in the dissipation range. Unfortunately, however, we have found no appropriate information to estimate the energy boundary condition for this separating flow. Therefore the boundary condition for the velocity has been introduced after Hanjalic & Launder (1972) or Launder *et al.* (1975).

Figure 4 shows a few typical examples of dimensionless velocity profiles for the interfacial region of the gas phase in the air–mercury flow. In the figure, the velocity and the distance from the interface are nondimensionalized by the interfacial friction velocities. The well known universal velocity profile is shown for comparison. In figure 4, a downward, nearly parallel shift from the universal velocity profile is observed with increasing gas phase Reynolds number. This trend corresponds to the remarkable increase of the interfacial shear stress, and is a well known characteristic of the rough wall turbulence.

For the turbulent flow over a rough wall, the velocity profile formula of the form

$$u^+ = \frac{1}{k} \ln \frac{y}{k_s} + B \qquad [46]$$

is widely applied. In [46], u^+ is the velocity divided by the friction velocity at the rough wall, κ is von Karman's universal constant, y is the distance from the wall, k_s is a roughness parameter and B is a constant depending on the roughness characteristics and the flow condition.

Based on this expression, the velocity profiles are re-plotted as in figure 5. In the figure, y is chosen as a distance from the interface and k_s is chosen as $\Delta h/2$. From this figure, B in [46] is nearly constant over the range of gas flow rate to which the present analysis refers. The solid line shows a correlation

$$u^+ = \frac{1}{0.4} \ln \frac{y - \delta}{\Delta h/2} + 5.2 . \qquad [47]$$

Therefore we use [47] as a "near-interface" condition to describe the turbulence structure in the gas phase. Consequently, the boundary conditions for the wavy interface are expressed using [45] and [47]. This means: for the liquid phase, the interfacial waves act as turbulence energy source: for the gas phase, the interfacial waves cause the flow separation. These boundary conditions make it necessary to modify the numerical procedure described before. This modification has to introduce some approximations using values obtained in the previous

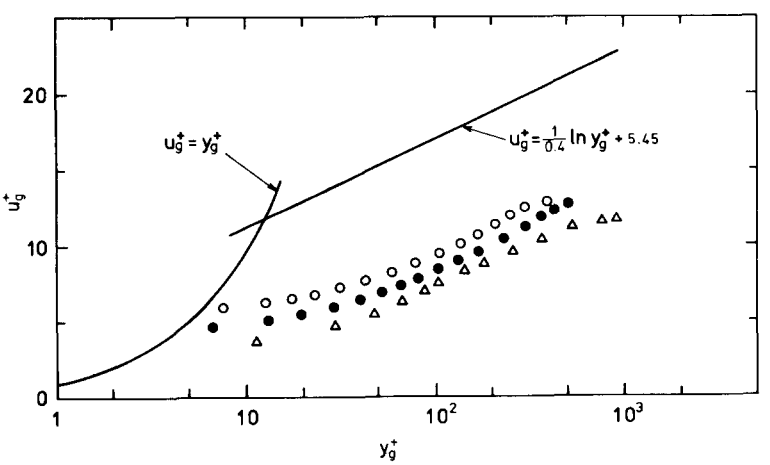

Figure 4. Mean gas velocity profiles for interfacial region. $Re_L = 8.04 \times 10^3$. ○, $Re_G = 6.25 \times 10^3$; ●, $Re_G = 8.54 \times 10^3$; △, $Re_G = 1.32 \times 10^4$; —, universal velocity profile.

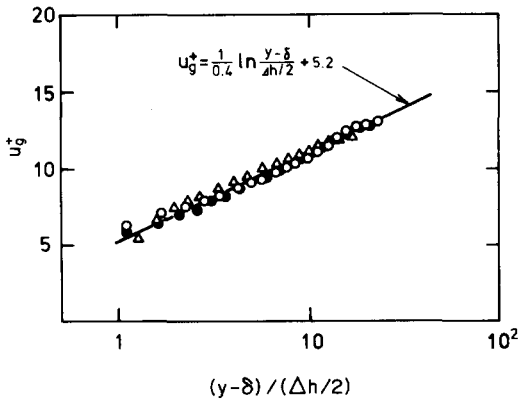

Figure 5. Rough surface correlation for gas velocity. $Re_L = 8.04 \times 10^3$; ○, $Re_G = 6.52 \times 10^3$; ●, $Re_G = 8.54 \times 10^3$; △, $Re_G = 1.32 \times 10^4$; —, correlation line.

computational step. But the final results are always satisfactory because the physical requirement, i.e. $\partial q/\partial t = 0$, is attained.

It is of course necessary to evaluate Δh and T in [44] and [47] in order to use these expressions. For this type of flow, however, there has been no useful theoretical approach to predict the structures of interfacial waves accurately. So we examined our experimental data and obtained the following empirical correlations

$$\frac{\Delta h}{2} = 7.38 \times 10^{-2} - 9.94 \times 10^{-6}\, Re_G + 7.36 \times 10^{-10}\, Re_G^2 \text{ (cm)}, \quad [48]$$

$$\frac{\Delta h}{T/2} = 3.68 - 2.47 \times 10^{-4}\, Re_G + 2.54 \times 10^{-8}\, Re_G^2 \text{ (cm/s)}, \quad [49]$$

$$\text{for } Re_L = 8.04 \times 10^3, \quad 5 \times 10^3 < Re_G < 1.6 \times 10^4.$$

The maximum error of these expressions is about 20%. We use [48] and [49] to determine the parameters in the boundary condition at the interface. The remaining unknown parameter β in [44] has been examined through the numerical optimization such that the calculated pressure drop and the liquid film thickness have agreed well with the experimental data. The resultant value for β is 0.50 under the present flow conditions. This value was the expected one and means that the turbulence energy at the interface can be well represented by the surface displacement velocity according to the definition of the turbulence kinetic energy.

The calculated liquid film thickness (holdup) and pressure drop are compared to the experimental results in figures 6 and 7. The numerical results for the smooth interface case are also shown by dashed lines and the notation "smooth" for reference. In figure 6, the present analysis for the wavy interface (notation "wavy") exhibits a better agreement with the experimental data than that for the smooth interface. However the improvement is not so significant as that for the pressure drop (figure 7). This is mainly due to the simple modelling of the turbulence energy at the interface. In figure 7, on the other hand, the effect of the rough interface is quite clear. The numerical results for the wavy interface explain well the tendency of the experimental data and the quantitative agreement is also quite good. The results for the smooth interface exhibit a poor prediction as the gas phase Reynolds number is increased.

In figures 8–10 the calculated velocity profiles and turbulence energy profiles are compared with the experimental data. Figures 8(a), 9(a) and 10(a) show the results for the gas phase. In these figures, the velocity and the distance from the interface are normalized by the maximum velocity and the gas phase thickness respectively. The solid and dashed lines denote the numerical results. The datum points compared with the turbulence energy show the streamwise

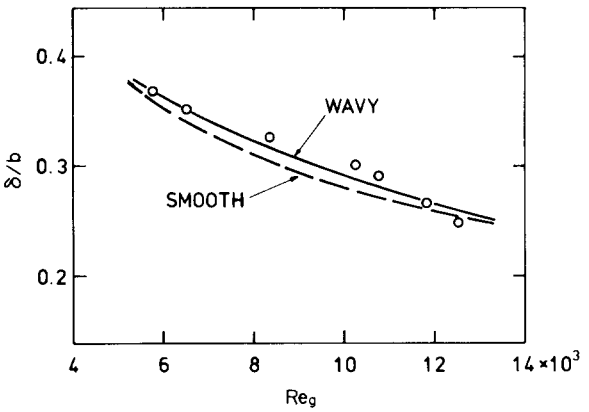

Figure 6. Liquid film thickness. $Re_L = 8.04 \times 10^3$. O, Experiment; - - -, prediction (smooth interface); —, prediction (wavy interface).

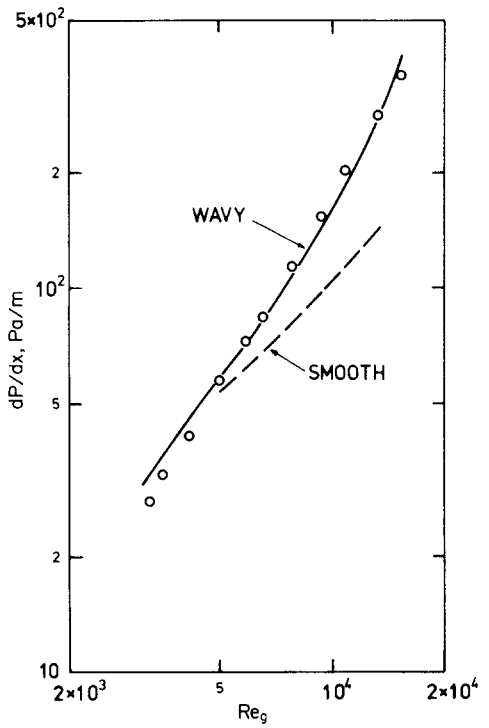

Figure 7. Pressure drop. $Re_L = 8.04 \times 10^3$. O, Experiment; - - -, prediction (smooth interface); —, prediction (wavy interface).

turbulence intensities ($\sqrt{(\overline{u'^2})}/u$), which can be considered to be proportional to the square root of the turbulence energy except for the region very close to the boundaries. This similarity between $\sqrt{(\overline{u'^2})}$ and $\sqrt{(k)}$ might be confirmed through the interpretation of the available data by Laufer (1953) for smooth wall turbulence and Hanjalic & Launder (1972) for rough wall turbulence. The results for the smooth interface are shown in figure 8(a), in which the numerical value has been obtained under the boundary conditions (12) and (13). The plane of the maximum velocity is located slightly below the central plane of the gas phase due to the moving interface at $y = \delta$. As can be seen from the figure, the velocity and the turbulence energy profile become nearly symmetric in the case of smooth interface. The wavy interface cases, on the other hand, show quite different results as shown in figures 9(a) and 10(a). The plane of the maximum velocity shifts toward the smooth lack of two lines indicated by [ ] in original paper page 29, that is [upper wall as the gas phase Reynolds number increased. These strongly asymmetric natures of the profiles cannot be explained by the analysis for the smooth] interface,

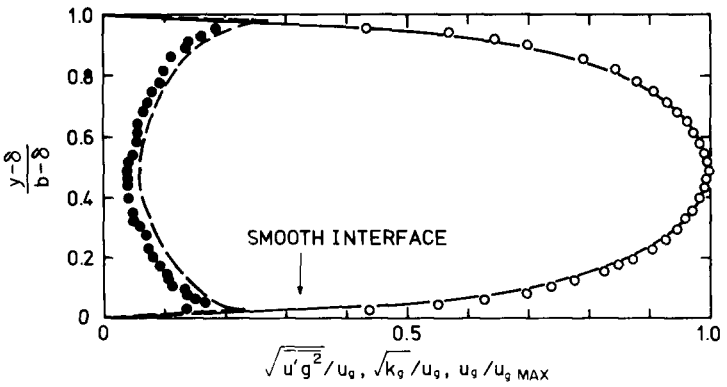

Figure 8(a).

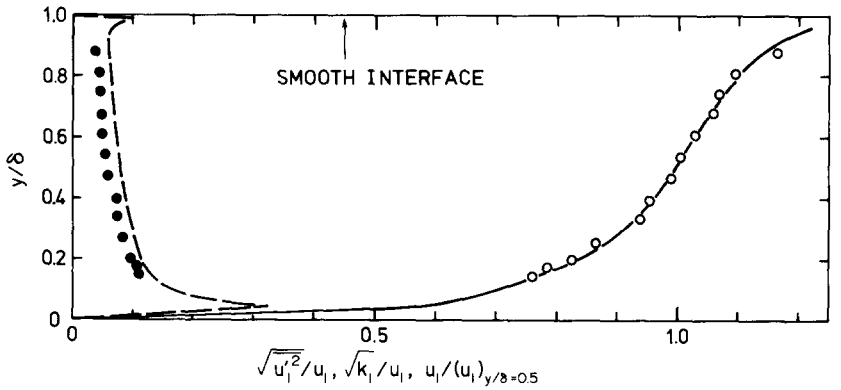

Figure 8(b).

Figure 8. Velocity and turbulent energy profile (smooth interface). $Re_L = 8.04 \times 10^3$, $Re_G = 2.34 \times 10^3$. Velocity profile: —, prediction; ○, experiment. Turbulent energy: - - -, prediction; ●, experiment (turbulent intensity). (a) Gas phase; (b) liquid phase.

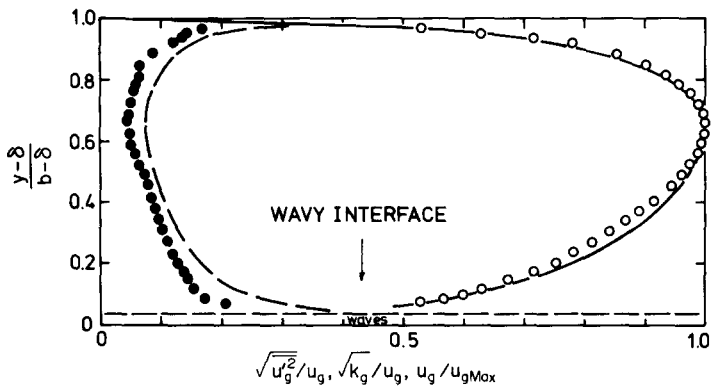

Figure 9(a).

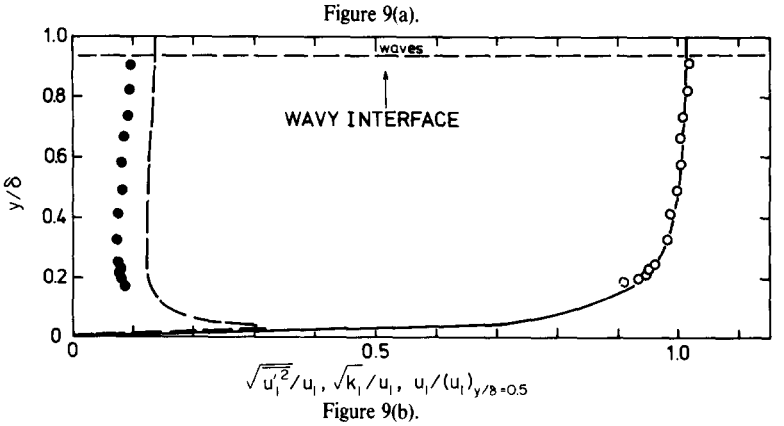

Figure 9(b).

Figure 9. Velocity and turbulent energy profile (wavy interface). $Re_L = 8.04 \times 10^3$, $Re_G = 6.52 \times 10^3$ (see figure 8 for notation).

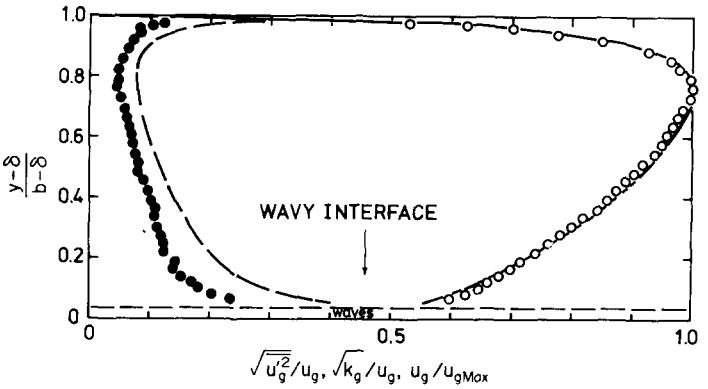

Figure 10(a).

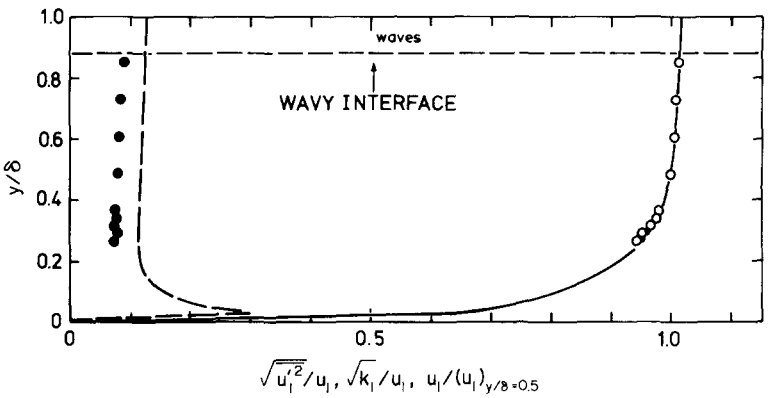

Figure 10(b).

Figure 10. Velocity and turbulent energy profile (wavy interface). $Re_L = 8.04 \times 10^3$, $Re_G = 1.32 \times 10^4$ (see figure 8 for notation).

and that is why the conventional analysis with smooth interface assumption underpredicts the pressure drop for the wavy flow regime. Both for smooth and wavy interface, the calculated velocity profiles agree well with the experimental data, and the measured profiles of the turbulence intensity are also satisfactorily reproduced by the analytical results for turbulence energy.

Figures 8(b), 9(b) and 10(b) show the results for the liquid phase. The distance from the lower wall is normalized by the liquid film thickness. The velocity at the plane $y/\delta = 0.5$ is chosen as a scaling value for the velocity profile. The results for the smooth interface are shown in figure 8(b). The value of $u_L/(u_L)_{y/\delta=0.5}$ at $y = \delta$ is 1.43. The velocity profile shows a well known nature of Couette flow due to the moving boundary at $y/\delta = 1$. On the other hand, the velocity profiles for the wavy interface are flattened ones (figures 9b and 10b), and indicate that a large amount of turbulent mixing should occur. This mechanism becomes clear from the turbulence energy profiles. The turbulence energy produced by the waves is transported progressively toward the bulk flow field. This phenomenon regarding the wave-induced velocity fluctuation was reported by Akai *et al.* (1977) for air-water system. As may be seen in these figures, the experimental results are fairly well explained by the present analysis.

4. CONCLUSIONS

The present work has attempted to analyze turbulent transport mechanisms in a horizontal, stratified two-phase flow with a two-equation model developed by Jones and Launder.

The effects of the interfacial waves on the flow field have been formulated in terms of the boundary conditions for the wavy gas-liquid interface. For the gas phase, the wavy interface has been considered to have a flow separation effect as a rough surface in a single-phase flow. For the liquid phase, the waves have been treated as a turbulence energy source. The numerical results taking into account these effects are in good agreement with the experimental

data for air–mercury system. Of course the physical considerations in the present analysis are yet by no means perfect. It must be emphasized that the turbulence structure in the separating flow over a rough surface has to become clear through the accumulation of detailed experimental data and the theoretical approach.

REFERENCES

AGGOUR, M. A. & SIMS, G. E. 1978 A theoretical solution of pressure drop and holdup in two-phase stratified flow. *Proc. Heat Transfer Fluid Mech. Inst.* 205–217.

AKAI, M., INOUE, A. & AOKI, S. 1977 Structure of a co-current stratified two-phase flow with wavy interface. *Theo. Appl. Mech.* **25**, 445–456.

AKAI, M., INOUE, A., AOKI, S & ENDO, K. 1980 A co-current stratified air-mercury flow with wavy interface. *Int. J. Multiphase Flow* **6**, 173–190.

AMES, W. F. 1965 *Non-linear Partial Differential Equations in Engineering.* Academic Press, New York.

DALY, B. J. & HARLOW, F. H. 1970 Transport equations in turbulence. *Phys. Fluids* **13**, 2634–2649.

ELLIS, S. R. & GAY, B. 1959 The parallel flow of two fluid streams: interfacial shear and fluid-fluid interaction. *Trans. Inst. Chem. Engrs* **37**, 206–213.

HANJALIĆ, K. & LAUNDER, B. E. 1972 A Reynolds stress model of turbulence and its application to thin shear flows. *J. Fluid Mech.* **52**, 609–638.

HANJALIĆ, K. & LAUNDER, B. E. 1976 Contribution towards a Reynolds-stress closure for low-Reynolds-number turbulence. *J. Fluid Mech.* **74**, 593–610.

HANRATTY, T. J. & ENGEN, J. M. 1957 Interaction between a turbulent air stream and a moving surface. *AIChE J.* **3**, 299–304.

JOHANNESSEN, T. 1972 A Theoretical solution of the Lockhart-Martinelli flow model for calculating two-phase flow pressure drop and hold-up. *Int. J. Heat Mass Transfer* **15**, 1443–1449.

JONES, W. P. & LAUNDER, B. E. 1972 The prediction of laminarization with a two-equation model of turbulence. *Int. J. Heat Mass Transfer* **15**, 301–314.

JONES, W. P. & LAUNDER, B. E. 1973 The calculation of low-Reynolds-number phenomena with a two-equation model of turbulence. *Int. J. Heat Mass Transfer* **16**, 1119–1130.

LAUFER, J. 1953 The structure of turbulence in fully developed pipe flow. NACA Rep. 1174.

LAUNDER, B. E., REECE, G. J. & RODI, W. 1975 Progress in the development of a Reynolds-stress turbulence closure. *J. Fluid Mech.* **68**, 537–566.

LOCKHART, R. W. & MARTINELLI, R. C. 1949 Proposed correlation of data for isothermal two-phase, two-component flow in pipes. *Chem. Engng Prog.* **45**, 39–48.